Microbial alignment in flow changes ocean light climate

Marcos[a,1], Justin R. Seymour[b,c,d,1], Mitul Luhar[b,1], William M. Durham[b,1], James G. Mitchell[c], Andreas Macke[e], and Roman Stocker[b,1,2]

[a]Department of Mechanical Engineering and [b]Ralph M. Parsons Laboratory, Department of Civil and Environmental Engineering, Massachusetts Institute of Technology, Cambridge, MA, 02139; [c]School of Biological Sciences, Flinders University, Adelaide, South Australia 5001, Australia; [d]Plant Functional Biology and Climate Change Cluster (C3), University of Technology, Sydney, Broadway, New South Wales 2007, Australia; and [e]Leibniz Institute for Tropospheric Research, Leipzig 04318, Germany

Edited by Jerry P. Gollub, Haverford College, Haverford, PA, and approved February 4, 2011 (received for review September 30, 2010)

The growth of microbial cultures in the laboratory often is assessed informally with a quick flick of the wrist: dense suspensions of microorganisms produce translucent "swirls" when agitated. Here, we rationalize the mechanism behind this phenomenon and show that the same process may affect the propagation of light through the upper ocean. Analogous to the shaken test tubes, the ocean can be characterized by intense fluid motion and abundant microorganisms. We demonstrate that the swirl patterns arise when elongated microorganisms align preferentially in the direction of fluid flow and alter light scattering. Using a combination of experiments and mathematical modeling, we find that this phenomenon can be recurrent under typical marine conditions. Moderate shear rates (0.1 s^{-1}) can increase optical backscattering of natural microbial assemblages by more than 20%, and even small shear rates (0.001 s^{-1}) can increase backscattering from blooms of large phytoplankton by more than 30%. These results imply that fluid flow, currently neglected in models of marine optics, may exert an important control on light propagation, influencing rates of global carbon fixation and how we estimate these rates via remote sensing.

rheoscopic | plankton

Sunlight attenuates as it passes through seawater, exerting a fundamental control on marine productivity by limiting the depth at which photosynthesis can occur (1–3). The extinction of sunlight is governed by the inherent optical properties (IOPs) of seawater, which are determined largely by the light-scattering characteristics of suspended living and nonliving microscopic particles (4). From a technological perspective, backscattered sunlight enables measurements of primary production rates and detection of phytoplankton blooms via remote sensing (3, 5). A major contribution to the IOPs comes from bacteria and phytoplankton (6), as a consequence of their size, pigment content, and high concentration (10^9–10^{13} m^{-3}). For example, phytoplankton larger than 3 μm were recently found to be responsible for 50% of the light backscattered in the open ocean (7). Although light scattering by marine particles is now computed routinely by optical models (4, 8), frequent discrepancies between predicted and measured IOPs highlight the need to better understand the complex underlying physics (6). Here, we demonstrate that fluid motion can alter the scattering characteristics of seawater by preferentially aligning elongated microbes, indicating that flow modulates the propagation of light through the ocean.

Intriguingly, the biophysical mechanism underlying this process is the same that underpins a method routinely used to assess microbial growth qualitatively in the laboratory. When liquid cultures of microorganisms are shaken within test tubes, visible millimeter-scale patterns often appear (Fig. 1*A*) almost instantaneously and persist for ∼1–5 s after shaking has ceased (Movie S1). We have observed these patterns in suspensions of several species of bacteria and phytoplankton. Patterns arise as translucent swirls and initially appear paradoxical, because they suggest that stirring causes locally enhanced cell concentrations rather than homogenizing the suspension. However, neither biological nor physical mechanisms can generate and dissipate cell accumulations so rapidly. The occurrence of patterns in cultures of nonmotile and dead cells rules out active congregation by cell motility, and neither sedimentation nor particle inertia is capable of producing aggregations of micrometer-scale organisms (9, 10).

Results and Discussion

Swirls in Culture Tubes. We examined the pattern-formation phenomenon by performing a classic fluid mechanics experiment. Towing a cylinder through a suspension of the bacteria *Pseudoalteromonas haloplanktis* revealed the well-known von Kármán vortices (11) (Fig. 1*B*). This observation indicates that the patterns reflect gradients in fluid velocity and that the microbial suspension acts as a rheoscopic ("flow-visualizing") fluid (12, 13). In rheoscopic fluids, hydrodynamic shear preferentially aligns elongated particles with the flow direction. Because optical scattering is a function of particle orientation (12, 13), particles aligned along different shear planes scatter light differently, mirroring the spatial distribution of shear in the flow. This assessment is supported by our observation that swirls form in test tubes containing rod-shaped and flagellated bacteria but not with the spherical cyanobacterium *Prochlorococcus* or with 1- to 5-μm spherical latex beads. Furthermore, when exposed to a vortex generated in a microfluidic device, *P. haloplanktis* displayed strong alignment with the flow streamlines (Fig. 1*A*, *Inset*).

A Mathematical Model Coupling Alignment by Shear with Light Scattering. To predict how light scattering by a microbial suspension is affected by shear-induced alignment and to determine the magnitude of this effect in the ocean, we developed a mathematical model that couples fluid dynamics and optics. In most ocean optics models particles are treated as spheres (6) or as randomly oriented spheroids (14–16). We model particles as prolate spheroids and explicitly compute their orientation distribution as a function of the shear rate, S (for example, the vertical gradient, du/dz, in horizontal fluid velocity, u). The particle's mean light-scattering properties then are calculated as a weighted average over all orientations. The probability distribution, $c(\theta, \phi)$, that the particle's major axis is oriented along polar and azimuthal angles (θ, ϕ) in a spherical coordinate system (17) is computed by solving the steady Fokker–Planck equation (18, 19),

Author contributions: M., J.R.S., M.L., W.M.D., J.G.M., and R.S. designed research; M., J.R.S., M.L., W.M.D., A.M., and R.S. performed research; M., J.R.S., M.L., W.M.D., and R.S. analyzed data; and M., J.R.S., M.L., W.M.D., and R.S. wrote the paper.

The authors declare no conflict of interest.

This article is a PNAS Direct Submission.

[1]M., J.R.S., M.L., W.M.D., and R.S. contributed equally to this work.

[2]To whom correspondence should be addressed. E-mail: romans@mit.edu.

This article contains supporting information online at www.pnas.org/lookup/suppl/doi:10.1073/pnas.1014576108/-/DCSupplemental.

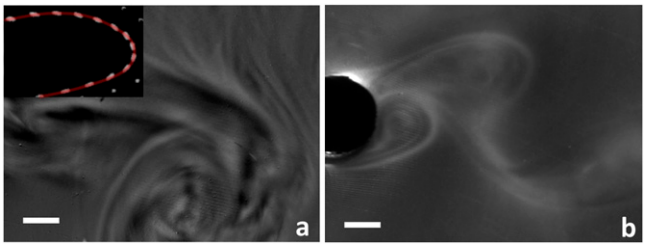

Fig. 1. Rheoscopic alignment produces optical patterns in microbial suspensions exposed to flow, revealing the underlying fluid motion. (*A*) A swirl induced by agitating a culture of *P. haloplanktis* bacteria. Such swirls provide microbiologists a means for rapidly assessing cell density in cultures. *P. haloplanktis* has a 1:10 aspect ratio, including the flagellum. (Scale bar: 3 mm.) See also Movie S1. (*Inset*) Multiple-exposure image showing alignment of *P. haloplanktis* with a streamline (in red) within a microfluidic vortex (25). The cell body is ~1 × 2 μm. (*B*) A von Kármán vortex street behind a cylinder towed through a suspension of *P. haloplanktis*. (Scale bar: 3 mm.)

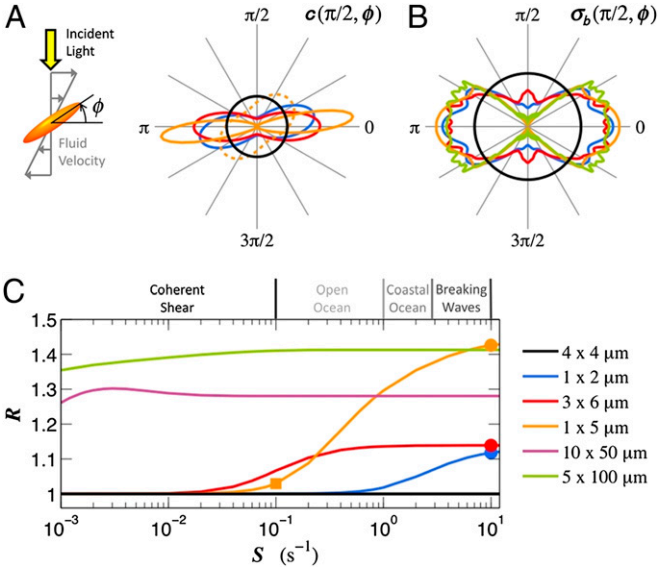

Fig. 2. A coupled fluid mechanics/optics model reveals that flow can affect the inherent optical properties of the ocean significantly. (*A*) Shear tends to align cells in the direction of flow. The probability distribution of particle orientation, $c(\pi/2,\phi)$, shows that alignment increases when cells are either larger or more elongated (see *C* for legend). The flow is along $\phi = 0$; the shear is along $\phi = \pi/2$. The dashed line shows results for $S = 0.1\ s^{-1}$ (square in *C*); solid lines are results for $S = 10\ s^{-1}$ (circles in *C*). The black line shows the case of a spherical particle (for any value of *S*). (*B*) Backscattering cross-section as a function of particle orientation, $\sigma_b(\pi/2,\phi)$. Incident light originates from $\phi = \pi/2$. Profiles are normalized so that they have equal area. (*C*) Flow increases optical backscattering for typical marine microorganisms. *R* is the mean backscattering cross-section of particles in a flow with shear rate *S*, normalized by the same quantity computed for $S = 0$ (for which particles assume random orientation). The departure of *R* from 1 results from the coupling of shear-induced alignment with the flow (*A*) and the orientation-dependence of scattering (*B*). The magnitude of this effect (i.e., $R-1$) depends on cell size, aspect ratio, and shear rate. Typical shear rates are shown above the panel for coherent flows (in black) and turbulent flows (in tones of gray).

$D\nabla^2 c - \nabla(\bar{\omega}\, c) = 0$, where D is the rotational diffusivity and $\bar{\omega}(\theta,\phi)$is the shear-induced particle rotation rate (*Materials and Methods*). The Fokker–Planck equation, which governs the degree of alignment of particles with the flow, parameterizes the competition between Brownian rotational diffusion and shear. The former randomizes cell orientation via stochastic collisions with water molecules, whereas the latter causes elongated particles to rotate with deterministic periodic orbits in which cells spend most of their time aligned with the flow. The time scale for a spheroid of aspect ratio r to align with the flow is $(r^2+1)/(rS)$ (*Materials and Methods*). The relative importance of shear and rotational diffusion is quantified by the Peclet number, $Pe = S/D$: Large Peclet numbers result in marked alignment, whereas low Peclet numbers yield random orientation. We found that shear rates characteristic of the marine environment can induce strong anisotropy in the orientation of particles of size and shape typical of marine microbes (Fig. 2*A*). For example, the proportion of time spent by a 1×5 μm spheroid within ±10° of the flow direction is seven times larger at $Pe = 100$ than in the case of isotropic orientation ($Pe = 0$).

Light scattering by a particle is quantified by its forward and backward optical scattering cross-sections, which measure the ratio of the rate by which energy of a plane parallel wave is scattered by the particle—in the forward and backward directions, respectively—to the incident irradiance on it (20). The total scattering is the sum of forward and backward scattering. We computed the total and backward scattering cross-sections, σ_{tot} and σ_b, for each orientation (θ, ϕ) and found them to be strongly orientation dependent (Fig. 2*B*). For example, a 1×5 μm spheroid aligned with the incident light has a 20-fold smaller σ_b than the same spheroid aligned in the perpendicular orientation. From knowledge of σ_{tot} and σ_b for each orientation, the mean scattering cross-sections, $\bar{\sigma}_{tot/b} = \int_0^{2\pi}\int_0^{\pi} \sigma_{tot/b}(\theta,\phi)c(\theta,\phi)\sin\theta\, d\theta\, d\phi$, then were computed as a weighted average over all particle orientations, with weights given by the probability distribution $c(\theta, \phi)$.

Rheoscopic Alignment and Light Transmission. We experimentally quantified the impact of shear on the optical properties of a microbial suspension by measuring the light transmitted through a culture of *Escherichia coli* bacteria exposed to shear in a Couette device (Fig. 3 and *Materials and Methods*). When a $2.9\ s^{-1}$ mean shear rate was applied, transmission of light through the bacterial culture increased considerably, whereas stopping the flow resulted in a return to the baseline transmissivity (Fig. 3). Relative to quiescent conditions, shear reduced the mean scattering cross-section of the bacteria by 16%. The increase in light transmission under shear might be surprising at first, because shear tends to align bacteria horizontally so that they expose more frontal area to the incident light. However, this effect arises because *E. coli* is comparable in size to the wavelength of light; the effect has been observed previously for red blood cells (21). Our mathematical model predicts a 13% decrease in the mean scattering cross-section, providing further confirmation that the change in transmittance was caused by a shear-induced modulation of optical scattering.

Effect of Rheoscopic Alignment in Aquatic Environments. We propose that preferential orientation of particles in flow (Fig. 2*A*) coupled with the dependence of scattering on orientation (Fig. 2*B*) can strongly influence the IOPs of the ocean (Fig. 4), because many planktonic microbes are elongated (14). Phytoplankton larger than 2 μm, for example, have a mean aspect ratio of ~5. We hypothesize that the orientation of elongated microbes is organized by temporally coherent shear flows produced by wind, currents, tides, fronts, or internal waves or by ephemeral turbulent shear. An important distinction needs to be made between coherent and turbulent shear. The latter often is stronger (up to $10\ s^{-1}$) (22) than the former (up to $0.1\ s^{-1}$) (23, 24) but varies in orientation over small distances (on the Kolmogorov scale, millimeters to centimeters) (22). In contrast, horizontal flows can produce coherent shear over meters to tens of meters of depth (23, 24). Therefore, the effect of turbulence on light scattering will be more pronounced locally, but coherent shear will yield a larger cumulative effect by inducing horizontal alignment of plankton (Fig. 4*B*) over considerably larger depths.

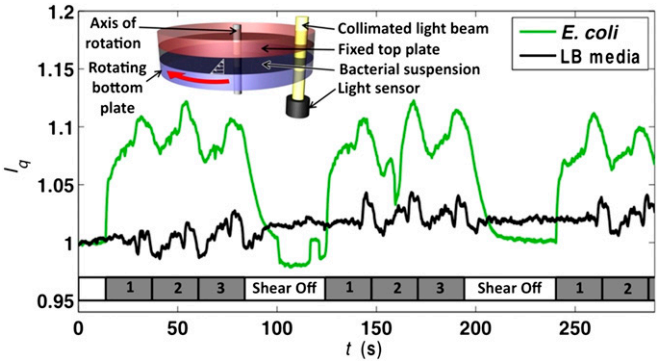

Fig. 3. Shear alters the transmission of light through microbial suspensions. The time series of normalized transmitted light intensity, I_q (*Materials and Methods*). Transmittance increases when shear in the *E. coli* suspension is initiated (green line) and decays when the shear is turned off. The asymmetry between the rapid ramp-up in I_q (~1–5 s) and the slower decay (~10–20 s) is in line with the known asymmetry in the spin-up versus spin-down times of fluid in cylindrical containers (30). Each gray segment indicates one revolution of the bottom plate. Control experiments performed in LB medium alone (black line) produced no appreciable difference in transmittance. Experimental noise in the calculation of I_q was ~0.03. (*Inset*) Diagram of the experimental set up. A collimated light beam was passed through a suspension of *E. coli* bacteria in LB medium sandwiched between two parallel plates. The top plate was held stationary, and the bottom plate was rotated at a constant rate for three revolutions, inducing shear within the fluid.

We computed light scattering by microorganisms of various shapes and sizes under typical marine shear rates (0.001–10 s^{-1}; Fig. 2*C*). Results show that large bacteria (1 × 2 μm spheroids) experience alignment only under strong turbulence ($S = 10\ s^{-1}$). Flagellated bacteria, having higher aspect ratio (1 × 5 μm), show an increase in backscattering of ~30% at $S = 1\ s^{-1}$. An increase in either size or elongation enhances the effect at small shear rates. Small phytoplankton (3 × 6 μm) exposed to moderate shear rates (0.2 s^{-1}) show a 10% increase in backscattering, whereas larger phytoplankton (10 × 50 μm) display an increase in backscattering of ~30% even at very low shear rates (0.001–0.01 s^{-1}).

Assemblages of multiple species were modeled by weighting the contribution of each species by its number density (*Materials and Methods*). We considered the case of seven microbial components, with sizes, number densities, and aspect ratios summarized in Table 1. Contrary to the dense cultures typical of laboratory experiments, this assemblage represents realistic microbial concentrations in the ocean. We found that a shear rate of $S = 0.1\ s^{-1}$ increases backscattering by 21% and total scattering by 13%, indicating that rheoscopic alignment can alter marine IOPs significantly. However, the effect of shear on light climate will vary with the local particle size and shape spectra. In this example, the primary contribution comes from ultra-nanoplankton and larger nanoplankton (Table 1). In general, optical scattering from smaller microbes (picoplankton), even when highly elongated (e.g., viruses), will not be altered by shear, because Brownian rotational diffusion, which is proportional to particle size to the power of −3 (*Materials and Methods*), renders orientation isotropic at typical marine shear rates. Scattering by spherical microbes also will be unaffected. The effect of this mechanism will be most pronounced when medium to large plankton (Fig. 2*C*), having large aspect ratio, are present in the water at high concentrations, such as during a bloom of an elongated or chain-forming phytoplankton species.

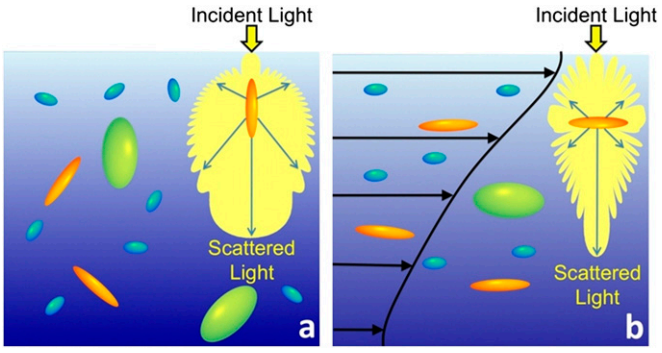

Fig. 4. Flow organizes the orientation of elongated microbes, thereby changing the fluid's bulk optical properties. (*A*) In quiescent conditions microbes are oriented randomly. (*B*) In a shear flow elongated organisms become preferentially aligned with the flow. Because optical scattering is strongly dependent on particle orientation, as shown by the two scattering profiles (yellow in *A* and *B*), this preferential alignment can affect the inherent optical properties of seawater.

Conclusions

These results indicate that a subtle interplay of biology, fluid dynamics, and optics may shape the light climate in aquatic systems. While rheoscopic alignment has long been part of the toolbox experimental fluid dynamicists use to visualize fluid flow, our findings suggest this phenomenon can also affect light propagation in the ocean. By altering the way that light is transmitted through the upper ocean (Fig. 4), fluid flow may have profound physical and biological consequences. Because the light climate plays a pivotal role in phytoplankton ecology, this phenomenon may exert a selection pressure on phytoplankton community composition and ultimately affect primary production levels by altering rates of light attenuation. Additionally, because remote sensing relies on the backscattering of light from ocean surface waters, shifts in IOPs driven by rheoscopic alignment may affect estimates of chlorophyll concentration obtained from satellite measurements of ocean color (5, 7). These results provide further evidence that biophysical interactions occurring at the microscale can play a key role in global scale marine processes.

Materials and Methods

Light Transmission Experiments. The nonflagellated *E. coli* strain VS115 was grown in LB medium to midexponential phase (OD_{600} = 0.42). Cultures were placed between two parallel circular Plexiglas plates (Fig. 3) spaced H = 5 mm apart. The upper plate was fixed, and the lower plate rotated at 0.5 Hz, producing a shear rate $S = 2.9\ s^{-1}$ at the measurement location. A collimated light beam (NI-150; Nikon) was passed vertically through the suspension, and the transmitted light was measured with a light meter (2832-C; Newport) and recorded at 25 Hz. The normalized intensity I_q was calculated by dividing the instantaneous intensity by the intensity under the initial quiescent conditions. To compute the change in scattering cross-section caused by shear,

Table 1. Equivalent diameter, concentration (N_i), and elongation of the seven components of a microbial assemblage used to quantify the change in backscattering induced by shear

Microbial component	Diameter (μm)	N_j (m^{-3})	Aspect ratio
Viruses	0.0715	3.0×10^{11}	1:10
Heterotrophic bacteria	0.53	3.0×10^{10}	1:2
Prochlorophytes	0.8	3.0×10^{8}	1:1
Cyanobacteria	1.3	3.0×10^{8}	1:1
Ultra-nanoplankton	3	3.0×10^{8}	1:5
Larger nanoplankton	11	4.5×10^{7}	1:5
Microplankton	28	3.0×10^{5}	1:1

Organisms were modeled as spheres (aspect ratio 1:1) or prolate ellipsoids (aspect ratios 1:2, 1:5, or 1:10). This table was modified from ref. 6.

$\Delta\bar{\sigma}_{tot}$, relative to quiescent conditions, we used Beer's law, $I_q = \exp(-\Delta\bar{\sigma}_{tot}NH)$, where N is the concentration of particles, and the definition of optical density is $10^{-OD} = \exp(-\bar{\sigma}_{tot}NH_{OD})$, where OD was measured separately in an H_{OD} = 0.8 mm wide cuvettete. Observation of more than 2,000 bacteria with an inverted microscope (TE2000; Nikon) showed that VS115 cells are 1.1 × 3.5 μm spheroids. Control experiments were performed with LB medium alone. The measurement error in I_q was ~0.03 and resulted primarily from small inhomogeneities in the Plexiglas surfaces.

Towed Cylinder Experiment. A 200-mL suspension of *P. haloplanktis* bacteria (cell body ~2 × 1 μm; ATCC 700530) grown in 1% Tryptic Soy Broth to midexponential phase (OD_{600} = 0.44) was placed in a 20 × 20 × 1 cm Perspex container. A cylinder 0.63 cm in diameter was towed through the 0.5-cm-deep bath of bacteria at 3.3 cm s^{-1}. Illumination was provided from underneath by an overhead projector, and images were captured from above at 25 Hz using a stereomicroscope (Nikon SMZ1000) and a CCD camera (PCO1600; Cooke).

Microfluidic Experiment. *P. haloplanktis* (grown as above) were imaged within a microfluidic vortex (25) using an inverted microscope (as above). Significant alignment with streamlines occurred at $S > 2.8\ s^{-1}$.

Coupled Model for Particle Orientation and Optical Scattering. To compute the scattering properties of a microbial suspension exposed to a constant, uniform shear rate, S, we coupled a probabilistic model of particle orientation to models that calculate the optical scattering induced by a spheroidal particle with arbitrary orientation. The probability density function of particle orientation, $c(\theta, \phi, t)$, is governed by the Fokker–Planck equation (18, 19), which expresses the balance between a deterministic "drift" process, here the rotational velocity of a spheroid $\bar{\omega}$ induced by shear, and a stochastic forcing, which in our case is the Brownian rotational diffusion of a spheroid (parameterized by its rotational diffusivity, D). Because we are interested in the long-term distribution of particle orientation, we compute the steady-state probability distribution, $c(\theta, \phi)$, by numerically integrating the steady Fokker–Planck equation using Multiphysics Modeling and Simulation Software (COMSOL).

The rotation rate of a spheroid, $\bar{\omega} = \dot{\phi}\hat{\mathbf{e}}_\phi + \dot{\theta}\hat{\mathbf{e}}_\theta$, in a flow with a constant, uniform shear rate is given by the well-known Jeffery's orbit equations (26),

$$\dot{\phi} = -\frac{S}{r^2+1}(r^2\sin^2\phi + \cos^2\phi)$$

$$\dot{\theta} = S(r^2-1)(\cos\theta\sin\theta\cos\phi\sin\phi)/(1+r^2),$$

where r is the aspect ratio of the spheroid (>1 for prolate spheroids), and θ and ϕ are the polar and azimuthal angles in a spherical coordinate system (identical to that used in ref. 17), with ($\theta = \pi/2$, $\phi = 0$) representing the flow direction and ($\theta = \pi/2$, $\phi = \pi/2$) representing the direction of shear. The Jeffery equations predict rapid rotation when the spheroid is aligned with the direction of shear and slow rotation when it is aligned with the flow direction.

The rotational diffusivity, D, was estimated using the Stokes–Einstein equation, $D = kT/F$, where F is the spheroid's torsional resistance, k is Boltzmann's constant, and T is temperature (20 °C). For a sphere of radius s, $F = 8\pi\mu s^3$, where μ is the dynamic viscosity of the fluid. For a spheroid, F is the torsional resistance in the direction perpendicular to its major axis (27),

$$F = \frac{16\pi\mu(b^2+a^2)}{3(b^2\,\beta_0 + a^2\,\alpha_0)},$$

where a and b are the half-major and half-minor axes, α_0 and β_0 are given by

$$\alpha_0 = -\frac{2}{e^2 a} - \frac{1}{e^3}\ln\frac{a-e}{a+e} \text{ and } \beta_0 = \frac{a}{e^2\,b^2} + \frac{1}{2e^3}\ln\frac{a-e}{a+e},$$

and $e = \sqrt{a^2-b^2}$ is the spheroid's eccentricity.

Optical scattering by a spheroid with arbitrary orientation with respect to the incident light was computed with the Extended Boundary Condition Method using the T-matrix code (17) for spheroids with equivalent spherical diameter <10 μm; for larger particles the Geometric Optics method (28) was used. The relative refractive index was assumed to be 1.05, appropriate for organic particles (14), and computations were performed for a wavelength of 550 nm. The direction of incident light was fixed at $\theta = \pi/2$, $\phi = 3\pi/2$. The T-matrix code (17) was used to compute the 4 × 4 scattering phase matrix, Z, of the spheroidal particle. For unpolarized incident light, the first element, Z_{11}, is the differential scattering cross-section, $\frac{d\sigma}{d\Omega} = Z_{11}$, a measure of the angular distribution of scattered light (29), where $d\Omega = \sin\theta\, d\theta\, d\phi$ is the differential integration area in spherical coordinates. The total (σ_{tot}) and backward (σ_b) scattering cross-sections of a particle with its long axis oriented along the direction (θ, ϕ) were calculated by integrating the differential cross-section Z_{11} over all possible directions for σ_{tot} and over all backward directions (with respect to the incoming light) for σ_b:

$$\sigma_{tot}(\theta,\phi) = \int_0^{2\pi}\int_0^{\pi}\frac{d\sigma}{d\Omega}\sin\theta\, d\theta\, d\phi$$

$$\sigma_b(\theta,\phi) = \int_0^{\pi}\int_0^{\pi}\frac{d\sigma}{d\Omega}\sin\theta\, d\theta\, d\phi.$$

The cumulative scattering coefficients produced by an assemblage of different species (i.e., different sizes and shapes) were computed by weighing the contribution of each species by its number density, Nj, as $b_b = \sum_{j=1}^{7} N_j\cdot(\bar{\sigma}_b)_j$, where subscript j refers to the j-th out of seven species.

Characteristic Timescale for Alignment in Shear. The angular velocity of a spheroid in a shear flow is given by $\dot{\phi} = -\frac{S}{r^2+1}(r^2\sin^2\phi + \cos^2\phi)$ (26), where for simplicity we assumed the spheroid to be aligned with the shear plane, i.e., $\theta = \pi/2$. Integrating with respect to time, one obtains $\tan\phi = -\frac{1}{r}\tan\frac{rSt}{r^2+1}$. This equation describes Jeffery orbits with period $2\pi(r^2+1)/(rS)$, and thus the characteristic timescale of alignment is $(r^2+1)/(rS)$.

ACKNOWLEDGMENTS. We thank Emmanuel Boss and John Cullen for comments on the manuscript, Henry Fu for discussions, and Thomas Shimizu for providing the *E. coli* strain VS115. This work was supported in part by Australian Research Council Grant DP0772186 (to J.R.S.) and by a Hayashi Grant from the Massachusetts Institute of Technology International Science and Technology Initiatives Program and by National Science Foundation Grant OCE-0744641-CAREER (to R.S.).

1. Ryther JH (1956) Photosynthesis in the ocean as a function of light intensity. *Limnol Oceanogr* 1:61–70.
2. Bisset WP, et al. (2001) Resolving the impacts and feedback of ocean optics on upper ocean ecology. *Oceanography (Wash DC)* 14:30–53.
3. Field CB, Behrenfeld MJ, Randerson JT, Falkowski P (1998) Primary production of the biosphere: Integrating terrestrial and oceanic components. *Science* 281:237–240.
4. Stramski D, Bricaud A, Morel A (2001) Modeling the inherent optical properties of the ocean based on the detailed composition of the planktonic community. *Appl Opt* 40: 2929–2945.
5. Sathyendranath S, Cota G, Stuart V, Maass H, Platt T (2001) Remote sensing of phytoplankton pigments: A comparison of empirical and theoretical approaches. *Int J Remote Sens* 22:249–273.
6. Stramski D, Kiefer D (1991) Light scattering by microorganisms in the open ocean. *Prog Oceanogr* 28:343–383.
7. Dall'Olmo G, Westberry TK, Behrenfeld MJ, Boss E, Slade WH (2009) Significant contribution of large particles to optical backscattering in the open ocean. *Biogeosci* 6:947–967.
8. Mobley CD, Stramski D (1997) Effects of microbial particles on oceanic optics: Methodology for radiative transfer modeling and example simulations. *Limnol Oceanogr* 42:550–560.
9. Jimenez J (1997) Oceanic turbulence at millimeter scales. *Sci Mar* 61:47–56.
10. Maxey MR, Corrsin S (1986) Gravitational settling of aerosol particles in randomly oriented cellular flow fields. *J Atmos Sci* 43:1112–1134.
11. Von Kármán T (1911) Über den Mechanismus des Widerstandes, den ein bewegter Körper in einer Flüssigkeit erfährt. 1. Teil. [On the mechanism of resistance experienced by a body moved in a fluid. Part 1]. *Gött Nachr* 509–517.
12. Savas O (1985) On flow visualization using reflective flakes. *J Fluid Mech* 152:235–248.
13. Hu D, Mendel L, Goreau T, Chan B, Bush JWM (2005) Visualization of a fish with Tobacco Mosaic Virus. Gallery of Fluid Motion. *Phys Fluids* 17:091103–1.
14. Clavano WR, Boss E, Karp-Boss L (2007) Inherent optical properties of non-spherical marine-like particles—from theory to observation. *Oceanogr Mar Biol Ann Rev* 45: 1–38.
15. Jonasz M (1991) Size, shape, composition, and structure of microparticles from light scattering. *Principles, Methods, and Application of Particle Size Analysis*, ed Syvitski JPM (Cambridge Univ Press, Cambridge, UK), pp 143–162.
16. Gordon HR (2006) Backscattering of light from disklike particles: Is fine-scale structure or gross morphology more important? *Appl Opt* 45:7166–7173.
17. Mishchenko MI (2000) Calculation of the amplitude matrix for a nonspherical particle in a fixed orientation. *Appl Opt* 39:1026–1031.
18. Risken H (1989) *The Fokker-Planck Equation* (Springer, Berlin).
19. Hill NA, Häder D-P (1997) A biased random walk model for the trajectories of swimming micro-organisms. *J Theor Biol* 186:503–526.

20. Bohren CF, Huffman DR (1983) *Absorption and Scattering of Light by Small Particles* (Wiley, New York).
21. Frojmovic MM, Okagawa A, Mason SG (1975) Rheo-optical transients in erythrocyte suspensions. *Biochem Biophys Res Commun* 62:17–24.
22. Lazier JRN, Mann KH (1989) Turbulence and the diffusive layers around small organism. *Deep-Sea Res* 36:1721–1733.
23. Dekshenieks MM, et al. (2001) Temporal and spatial occurrence of thin phytoplankton layers in relation to physical processes. *Mar Ecol Prog Ser* 223:61–71.
24. Ryan JP, McManus MA, Paduan JD, Chavez FP (2008) Phytoplankton thin layers caused by shear in frontal zones of a coastal upwelling system. *Mar Ecol Prog Ser* 354:21–34.
25. Marcos, Stocker R (2006) Microorganisms in vortices: A microfluidic setup. *Limnol Oceanogr Methods* 4:392–398.
26. Jeffery GB (1922) The motion of ellipsoid particles in a viscous fluid. *Proc R Soc A* 102: 161–179.
27. Steinberger B, Petersen N, Petermann H, Weiss DG (1994) Movement of magnetic bacteria in time-varying magnetic fields. *J Fluid Mech* 273:189–211.
28. Macke A, Mishchenko MI (1996) Applicability of regular particle shapes in light scattering calculations for atmospheric ice particles. *Appl Opt* 35:4291–4296.
29. Mishchenko MI, Travis LD, Lacis AA (2002) *Scattering, Absorption, and Emission of Light by Small Particles* (Cambridge Univ Press, Cambridge, UK).
30. Benton ER, Clark A, Jr. (1974) Spin-up. *Annu Rev Fluid Mech* 6:257–280.